View metadata, citation and similar papers at core.ac.uk
brought to you by CORE
provided by CiteSeerX

Proceedings of HT2003
ASME Summer Heat Transfer Conference
July 21-23, 2003, Las Vegas, Nevada, USA

HT2003-47141

# OPTIMAL DESIGN OF COMPACT HEAT EXCHANGERS BY AN ARTIFICIAL NEURAL NETWORK METHOD

**Rongguang Jia**
Rongguang.Jia@vok.lth.se

***Bengt Sundén**
Bengt.Sunden@vok.lth.se

Division of Heat Transfer, Lund Institute of Technology,
P.O. Box-118, Lund 22100, Sweden

## ABSTRACT

The artificial neural network (ANN) methods are introduced (mainly for calculation of thermal and hydraulic coefficients) into a computer-aided design code of compact heat exchangers (CCHE). CCHE integrates the optimization, database, and process drawing into a software package. In the code, a strategy is developed for the optimization of compact heat exchangers (CHEs), which is a problem with changeable objective functions and constraints. However, the applicability and/or accuracy of all these methods are limited by the availability of reliable data sets of the heat transfer coefficients ($j$ or $Nu$) and friction factors ($f$) for different finned geometries. In fact, due to expenses and difficulties in experiments, only a limited number of experiments has been carried out for some kinds of heat transfer surfaces. The information, therefore, is usually given by means of correlations. It is well known, however, that the errors in the predicted results by means of correlations are much larger than the measurement errors, being mainly due to the data reduction represented by them. This implies doubts on the optimal solutions. Fortunately, a well-trained network is capable of correlating the data with errors of the same order as the uncertainty of the measurements. This is the main reason for the present introduction of the ANN method to correlate the discrete experimental data sets into continuous formulas. In this study, the ANN method is used to formulate the complex relationship between the thermal and hydraulic coefficients and the other parameters, including the geometry and process data. A specific case on the optimal analysis of a plate-fin heat exchanger (PFH) is presented to show how the trained ANNs can be used for optimal design of heat exchangers. In addition, a case is presented to illustrate how an inverse heat transfer problem is solved by the optimization methodology developed in the present code.

## NOMENCLATURE

| | |
|---|---|
| $A$ | Heat transfer area |
| $b$ | Bias |
| $c_p$ | Specific heat |
| $C$ | Annual cost |
| $C_A$ | Price of one $m^2$ Heat transfer surface |
| $C_I$ | Investment annual cost |
| $C_O$ | Operation annual cost |
| $C$ | Annual cost |
| $f$ | Fanning friction factor |
| $F$ | Square of the temperature unevenness |
| $G$ | Mass flow velocity $\frac{M}{A}$ |
| $h$ | Heat transfer coefficient |
| $H$ | Fin height |
| $I$ | Input or Index I |
| $j$ | Colburn factor, $StPr^{2/3}$, or Subscript |
| $k_{el}$ | Price of electrical energy |
| $L$ | Strip length |
| $M$ | Mass flow rate |
| $O$ | Output |
| $P$ | Fin pitch, or Pressure |
| $Pr$ | Prandtl number |
| $\Delta P$ | Pressure drop |
| $Q$ | Heat transfer rate |

*Address all correspondence to this author.



Copyright © 2003 by ASME

Downloaded From: https://proceedings.asmedigitalcollection.asme.org on 06/29/2019 Terms of Use: http://www.asme.org/about-asme/terms-of-use

| | |
|---|---|
| $Re$ | Reynolds Number $\frac{\rho UD}{\mu}$ |
| $S$ | Weighted sum |
| $T$ | Target vector, Temperature, or Fin thickness |
| $T_i$ | Inlet temperature |
| $T_o$ | Outlet temperature |
| $U$ | Overall heat transfer coefficient |
| $V_t$ | Volumetric flow rate |
| $W$ | Weight |

**Greek symbols**

| | |
|---|---|
| $\alpha^*$ | Amortization |
| $\eta_0$ | Overall efficiency of the heat transfer area |
| $\eta_P$ | Efficiency of the pump |
| $\tau$ | The hours of operation per year |

**Subscripts**

| | |
|---|---|
| $c$ | The cold fluid side |
| $h$ | The hot fluid side |
| $i$,$J$ | The low-I surface of the element $I$,$J$ |
| $I$,$J$ | The element $I$,$J$ |

## INTRODUCTION

Compact heat exchangers (CHE) include plate-fin (PF) heat exchangers and plate heat exchangers, which are characterised by hydraulic diameters between 1 and 10 mm. They are complex devices used in a wide variety of engineering applications, e.g. automotive, aerospace, air-conditioning and refrigeration, as well as in electronic equipment industries for single phase and phase change duties. The complexity of these systems is due to their geometrical configuration, the physical phenomena present in the transfer of heat and to the large number of variables involved in its operation. These and the related physical processes increase the difficulty of solving the governing equations based on a first-principles approach. As a consequence, experimental information of the heat transfer coefficients and pressure drop as functions of the variables of the system must be determined experimentally, usually by the manufacturer, and presented to the user, i.e. the design engineer. Such information is usually given by means of correlations. These, however, have very little physical bases and are usually created to have the simplest form that will give the best accuracy. It is well known, however, that prediction errors in the heat transfer coefficients and pressure drop by means of correlations are much larger than the measurement errors, being mainly due to the data compression represented by them.

The problem of single-phase and condensing heat exchanger predictions has been previously addressed using artificial neural networks (ANNs) [1]. This is a technique that allows the modeling of physical phenomena in complex systems without requiring explicit mathematical representations. ANNs have been developed in recent years and used in many application areas, including thermal engineering [2]. Some examples are: analysis of thermosyphon solar water heaters [3], heat transfer data analysis [4], HVAC computations [5], predictions of critical heat flux [6], predictions of aerodynamic coefficients [7], predictions of thermal dynamic properties [8] [9].

In the present study we are interested in employing the ANN method to the prediction of the heat transfer coefficients and pressure drop in the optimization of plate-fin heat exchangers. To this end, we will use typical experimental data provided from the available literature. Firstly, the ANN approach will be applied to the data to show its capability in the representation of the thermal hydraulic coefficients. Secondly, the proposed technique will be applied to the available experimental measurements to confirm the validity of the method, and the error will be estimated. Finally, the validated ANN system is coupled to the optimization of a plate-fin heat exchanger, and the solution of a inverse heat transfer problem.

## METHODS

### Neural Network Methodology

ANN consists of large numbers of computational units connected in a parallel structure. The processing units (neurones) from each layer $n$ are linked to all of the other processing units appearing in layer $n+1$ by weighted connections. Collectively, these connections (as well as the transfer functions of the processing units) form more or less good distributed representations of relationships between input and output data. Neural networks do not need an explicit formulation of the mathematical or physical relationships of the handled problem. The input layer of the network (see Fig. 1) does not perform any processing, but acts as a means to introduce scaled data to the network. The data from the input neurones are propagated through the network via the interconnections. Every neurone in a layer is connected to every neurone in adjacent layers. A scalar weight is associated to each connection. The neurones within the hidden layer perform two tasks: they sum the weighted inputs connected to them and then pass the resulted summations through a non-linear activation function to the output neurone or adjacent neurones of the corresponding hidden layer (in case of more than one hidden neurone layer). In this work, the sigmoid function: $f(x) = 1/(1+e^{-x})$ is used in the interval (0.1, 0.9). A bias term is associated with each interconnection in order to introduce a supplementary degree of freedom.

The expression of the weighted sum to the $k^{th}$ neurone in the $j^{th}$ layer ($j \geq 2$) is given by

$$S_k^j = \sum_{i=1}^{N_{j-1}} (W_{i,k}^{j-1} I_i^{j-1}) + b_k^j \qquad (1)$$


Copyright © 2003 by ASME

Downloaded From: https://proceedings.asmedigitalcollection.asme.org on 06/29/2019 Terms of Use: http://www.asme.org/about-asme/terms-of-use

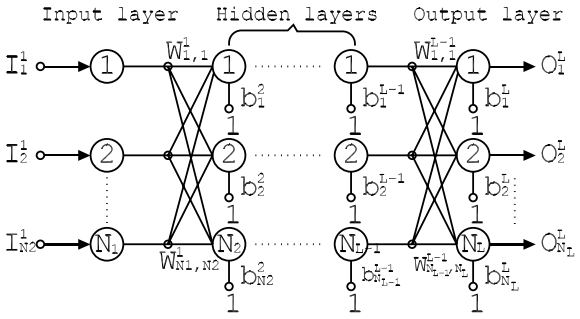


Figure 1. A feed-forward artificial neural network architecture

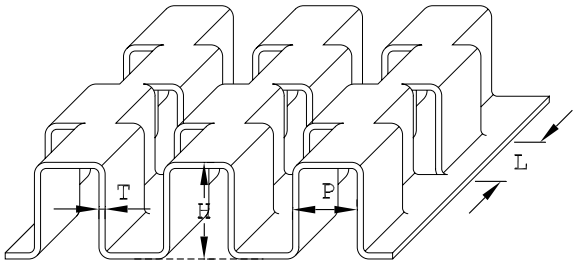


Figure 2. Schematic view of a strip fin

where $I_i^{j-1}$ is the output from the $i^{th}$ neurone in the $(j-1)^{th}$ layer, $b_k^j$ the bias term and $N^{j-1}$ is the number of neurones in the layer $j-1$.

The output of the $k^{th}$ neurone in the layer $j$ ($j \geq 2$) is

$$O_k^j = \frac{1}{1+exp(-S_k^j)} \tag{2}$$

An important aspect of a neural network is the learning step, based on a set of measured numerical values (the learning database). Representative examples are presented to the network so that it can integrate this knowledge within its structure. The accuracy of model representation depends directly on the topology of the neural network. Numerous papers have shown that a feed-forward network is potentially able to approximate any non-linear function. More details about neural networks are given in Hagan et al. [10]. The learning process consists of identifying the weights $W_{i,k}^j$ and $b_k^j$ which produce the best fit of the output data over the entire training data set. In this work, only one hidden layer has been considered. At the beginning of the learning step, random values are chosen to initialize weight data. During the learning step, the weights of the network are continuously adjusted, based on the error signal generated by the deviation between the output data computed through the network ($O^L$) and the data from the database used in the training examples (target vector $T$). This is accomplished by means of the learning algorithm-the back propagation algorithm-designed to minimize the least square total output error given by the objective function $F$:

$$F = \frac{1}{2}\sum_{i=1}^{N_T}\sum_{k=1}^{N_L}(T_k(i) - O_k^L(i))^2 \tag{3}$$

$N_T$ is the number of training data set, $N_L$ corresponds to the number of outputs of the neural network, $T_k$ represents the target value corresponding to the $k^{th}$ neurone of the output layer and $O_k^L$ the calculated value corresponding to the $k^{th}$ neurone of the output layer. The deviations between network outputs and targets are summed over the entire data set and updating of the weights is performed after every presentation of the complete data set. This procedure is iterated until a converged solution is reached.

## ANN Design for the Analysis of Thermal Hydraulic Data

In this work, and for both thermal and hydraulic parameters, the neural models are devoted to the computation of the heat transfer coefficients ($j$) and friction factors ($f$) (output neurone), as function of fin geometry parameters (pitch, height, thickness, and etc.) and Reynolds number ($Re$) (input neurones of the input layer). For example, the parameters, for a strip fin as shown in Fig. 2, are the fin thickness ($T$), fin height ($H$), fin pitch ($P$), strip length ($L$), and Reynolds number ($Re$). One hidden layer has been considered.

The number of nodes on the hidden layer determines a networks's ability to learn the intended function from the training data and to generalize it to new data. If a neural network has too many hidden neurons, it will almost exactly learn, or memorize, the training examples, but it will not perform well in recognizing new data after the training process is complete. If a neural network has too few hidden neurons, it will have insufficient memory capacity to learn a complicated function represented by the training examples, i.e., the data will be under-fitted, as stated by Rajkumar et al. [7]. The optimized number of hidden neurons has been determined during the learning phase by trial and error tests. Two neural network models are elaborated for $j$ and $f$ separately.

In order to improve the approximation capabilities of the feed-forward neural networks, the availability of sufficiently large and representative training data well distributed over the fin parameters and $Re$ domains, usually ensures good generalization properties of the trained neural networks. We collected data for training or testing purposes from the book by Kays and London [13], for plain, strip, wavy, and louvered fins.


Copyright © 2003 by ASME

Downloaded From: https://proceedings.asmedigitalcollection.asme.org on 06/29/2019 Terms of Use: http://www.asme.org/about-asme/terms-of-use

Table 1. Thermal parameters in the heat exchanger design problem.

| | Sizing Problem | Rating Problem |
|---|---|---|
| $UA$ | N | Y |
| $[Mc_p]_h$ | Y | Y |
| $[Mc_p]_c$ | Y | Y |
| $T_{i,h}$ | * | Y |
| $T_{o,h}$ | * | N |
| $T_{i,c}$ | * | Y |
| $T_{o,c}$ | * | N |
| $Q$ | N | N |

Y - Known, N - Unknown.

* - Three of these are known.

## Design of Compact Heat Exchangers

Nearly all heat exchangers can be analyzed from the following basic design equations:

$$Q = UA\Delta T \tag{4}$$

$$Q = [Mc_p(T_i - T_o)]_h = [Mc_p(T_o - T_i)]_c \tag{5}$$

where $\Delta T$ is a suitable temperature difference, depending on heat exchanger type, flow rates, and actual temperatures. There are eight variables in the above equations, as shown in Tab. 1. In order to solve these equations, five of them have to be given.

In CCHE, the $\varepsilon - NTU$ method (Kays and London [13]) is employed to solve the thermal equations. In the design of a CHE, the data of heat transfer and friction factors are required for various heat transfer surfaces, which made the solving procedure complex, unlike shell-and-tube heat exchangers (STHE). In a previous study [12], these factors were calculated with data queries from the database or empirical correlations. However, in this work, they are feeded by the trained ANN which provides the relation among $Re$, $j$, $f$, and fin geometry.

# RESULTS

## Validation of the Neural Network

Four type of fin geometries are studied in this work, namely, plain, strip, louver, and wavy, where the experimental data are obtained from the book of Kays and London [13]. For the plain, strip, and louver fins, half of the data (every second of the fins shown in Tab. 2) are selected for the learning process, and the left data are used for the test purpose. However, all the data for wavy fins are employed for the learning process, because only three kinds of wavy fins are available.

Table 2. Fins employed in the present study.

| plain | strip | louver | wavy |
|---|---|---|---|
| 5.3 | 1/2-11.94(D) | 1/2(a)-6.06 | 11.44-3/8W |
| 6.2 | 1/4-15.4(D) | 1/2-11.1 | 11.5-3/8W |
| 9.03 | 1/6-12.18(D) | 1/2-6.06 | 17.8-3/8W |
| 10.27T | 1/7-15.75(D) | 1/4(b)-11.1 | |
| 11.1 | 1/8-13.95 | 1/4-11.1 | |
| 11.11(a) | 1/8-15.2 | 3/16-11.1 | |
| 11.94T | 1/8-16.00(D) | 3/4(b)-11.1 | |
| 12.00T | 1/8-16.12(D) | 3/4-11.1 | |
| 14.77 | 1/8-16.12(T) | 3/8(a)-6.06 | |
| 15.08 | 1/8-20.06(D) | 3/8(a)-8.7 | |
| 16.96T | | 3/8(b)-11.1 | |
| 19.86 | | 3/8-11.1 | |
| 25.79T | | 3/8-6.06 | |
| 30.33T | | 3/8-8.7 | |

**Ability to Fit the Experimental Data** Figure 3 shows the comparison between the experimental Fanning friction factors and those computed by the ANN models for a learning data base for the plain fins. It is clear that the ANN model gives an accurate representation of the Fanning friction factors over the full operating conditions. Even better prediction by the ANN for the wavy fins can be observed, as shown in Fig. 4. Similar levels of accuracy are obtained for the other types of fins and the heat transfer factor j, so they are not shown here.

**Ability in Predicting the Thermal and Hydraulic Data** The trained ANNs for the plain fins are used to predict the data sets which are reserved for the test purpose, and the prediction errors made by ANN on the test data are shown in Fig. 5 as an error frequency distribution histogram. It is interesting to observe that the error distribution is nearly Gaussian. The average errors, and the RMS errors of the distribution are 1.4%, 11.1% for $f$, and 1.5%, 5.5% for $j$, respectively.


Copyright © 2003 by ASME

Downloaded From: https://proceedings.asmedigitalcollection.asme.org on 06/29/2019 Terms of Use: http://www.asme.org/about-asme/terms-of-use

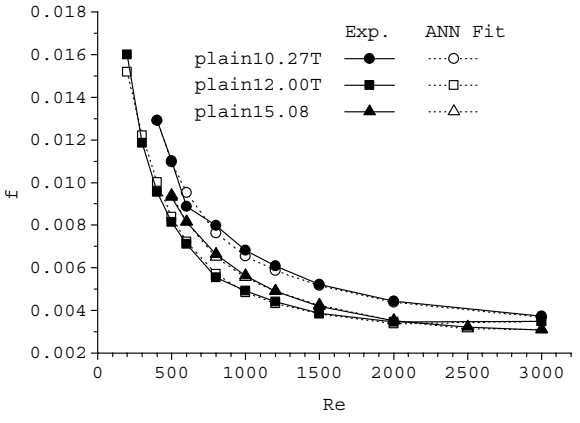


Figure 3. Friction factor of the plain fins

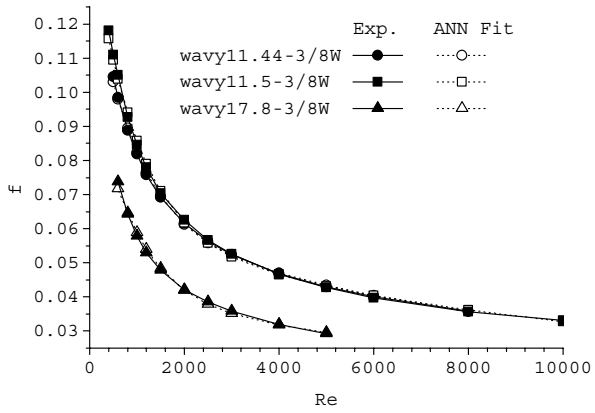


Figure 4. Friction factor of the wavy fins

**Check of Over-fitting** An important step in validating the network is to check the over-fitting problem, which could appear due to too many hidden layers or neurons. In this case, 400 input sets, which are different in Reynolds number, were generated for the fin `wavy11.44-3/8W`. The test results are shown in Fig. 6. As can be observed, there is no fluctuation or over-fitting at all, which means the number of the hidden layer neurons is not excessive. Similar tests are performed on the other trained ANNs, and there is no over-fitting found.

## Optimal Design of a Plate-Fin Heat Exchanger

The trained ANNs are employed in the study of the plate-fin heat exchangers, which is an extension of the work presented in Jia et al. [12]. The sketch of the heat exchanger core is shown

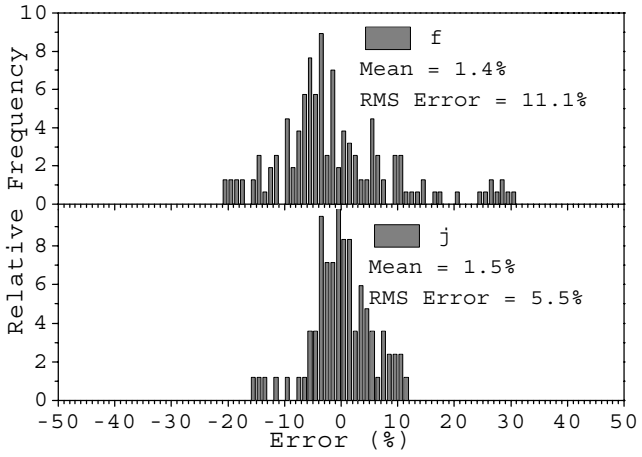


Figure 5. The rms errors of the predictions of the test data by the trained ANNs

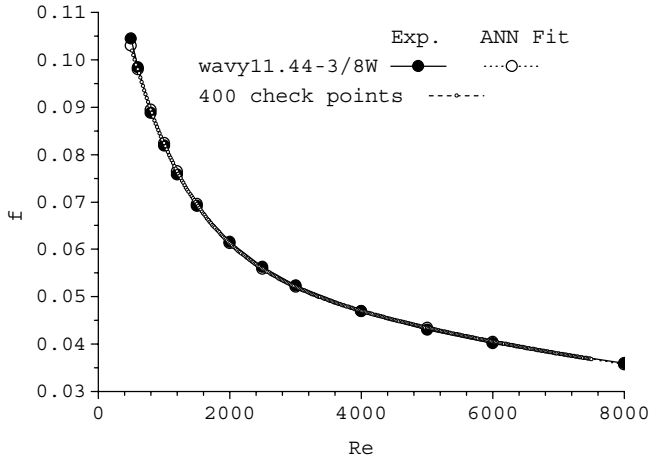


Figure 6. Check of over-fitting

in Fig. 7. The thermal and hydraulic parameters of the targeted heat exchanger is shown in Tab. 3, and more detailed specifications can be found in Jia et al. [12]. The present trained ANNs enabled the possibility of the optimization of plate-fin heat exchanger based on the available experimental data set, and a detailed study of the effect of the fin geometries. In this study, the pressure drops on both side are set as optimization variables. This was proved to be important in the previous studies.


Copyright © 2003 by ASME

Downloaded From: https://proceedings.asmedigitalcollection.asme.org on 06/29/2019 Terms of Use: http://www.asme.org/about-asme/terms-of-use

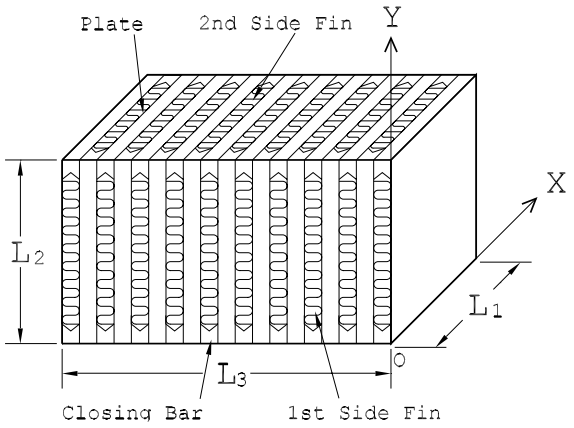


Figure 7. Schematic view of a cross-flow PF core

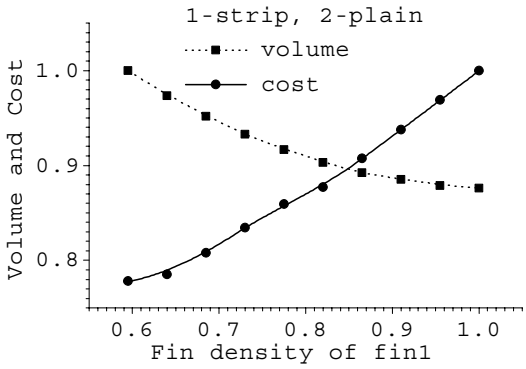


Figure 8. The variation of the objective functions with the 1st side fin density, where both the x- and y-axes are normalized

**Cost Function** The annual cost, including the initial investment and operation cost, is modelled as follows:

$$\begin{aligned} C &= C_I + C_O \\ C_I &= C_A A \alpha^* \\ C_O &= \left( k_{el} \tau \frac{\Delta p V_t}{\eta_p} \right)_h + \left( k_{el} \tau \frac{\Delta p V_t}{\eta_p} \right)_c \end{aligned} \tag{6}$$

The annual costs of investment $C_I$ or capital costs are taken to be proportional to the surface area A and the amortization $\alpha^*$ (of say $10\%/yr$). The price per unit area $C_A$ depends of course on the type of apparatus, on the material needed, and on the size (i.e., on the surface area $A$) itself. It is generally well known that the price of equipment is not linearly increasing with its size. Thus $C_I$ in Eq. 6 should be regarded as a linearization of a more appropriate empirical power law (e.g., $C = Const \cdot A^n$), with an exponent $n$ less than unity.

Table 3. Heat exchanger process parameters.

| | 1st Side | 2nd Side |
|---|---|---|
| Initial Fin Type | strip1/8-16.00(D) | plain19.86 |
| Working Fluid | Air | Gas |
| Mass flow rate (kg/s) | 0.8296 | 0.8962 |
| Temperature, Inlet ($^o$C) | 4 | 240 |
| Temperature, Outlet ($^o$C)* | 199.8 | 61.4 |
| Pressure, Inlet (kPa) | 110 | 110 |
| Allowable pressure drop (kPa)# | 1.67 | 0.32 |
| Heat duty (kW) | 166.886 | |

* One of the two outlet temperatures is known.

# Allowable pressure drops can be optimization variables.

The cost of operation $C_O$ for heat exchangers with process fluids on both sides is taken as proportional to the pumping power required to overcome the flow resistances in the exchanger. It depends on the following variables: the price of electrical energy $k_{el}$, the hours of operation per year $\tau$, the pressure drop $\Delta p$, the volumetric flow rate $V_t$, and last but not the least, the efficiency of the pump (or fan) $\eta_p$.

**The Effect of the 1st Side Fin Density** Figure 8 shows the variation of the normalized core volume ($L_1 L_2 L_3$) and annual cost ($C$) with the normalized fin density, i.e., the fin number per unit length. As shown, the volume of the heat exchanger core will decrease with the increase of the fin density. This is so because the increase of the fin density results in a higher compactness of the fin, and consequently a smaller core size. However, the increase of the fin density will increase the pressure drop used to maintain the working fluid flow. This increase of pressure drop definitely results in a higher annual cost, including the capital cost and operation cost. Therefore, it is a compromise to get the the optimal fin density, which depends on the weights of the core volume and annual cost.

**The Effect of the 1st Side Fin Height** Figure 9 shows the variation of the normalized core volume and annual cost with the normalized fin height of the 1st side. As shown, both the annual cost and core volume follow a similar trend with variation of the fin height. This makes the selection of the optimal fin height straightforward, which is around 0.55. With the in-


Copyright © 2003 by ASME

Downloaded From: https://proceedings.asmedigitalcollection.asme.org on 06/29/2019 Terms of Use: http://www.asme.org/about-asme/terms-of-use

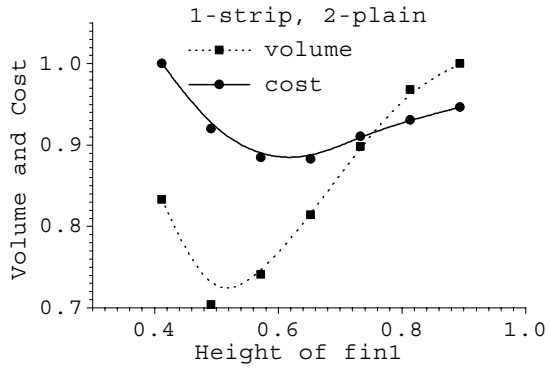


Figure 9. The variation of the objective functions with the 1st side fin height, where both the x- and y-axes are normalized

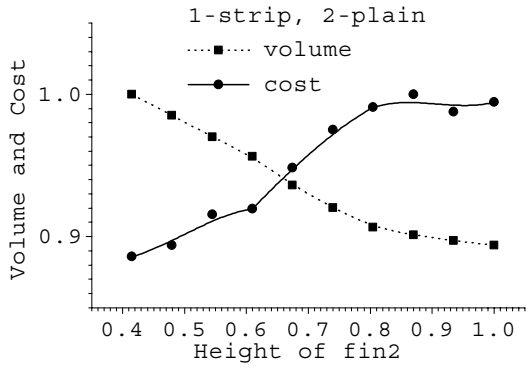


Figure 10. The variation of the objective functions with the 2nd side fin height, where both the x- and y-axes are normalized

crease of the fin height, the friction will be lower, so that the heat exchanger can operate at a higher Reynolds number, which results in a higher heat transfer coefficient. Consequently, less heat transfer area, smaller size, and less cost are obtained. However, if the fin height is further increased, the fin efficiency will decrease fast. This is not a good feature for heat transfer. Therefore, the cost and core size will increase again.

**The Effect of the 2nd Side Fin Height** Figure 10 shows the variation of the normalized core volume and annual cost with the normalized fin height of the 2nd side. The change of the core volume and annual cost follow different directions with the increase of 2nd side fin height. The decrease of the core volume is due to the friction factor decrease with increasing fin height. Similar to the increase of the 1st side fin height, higher Reynolds number can be employed on this side, which results in a smaller heat transfer area, and consequently a smaller core size. Because plain fins are used, there are no elements to breakup the boundary layer, so that a large Reynolds number is needed in order to provide sufficient heat transfer coefficients. This higher Reynolds number requires a high pressure drop, which results in a high operation cost.

## Solution of an Inverse Heat Transfer Problem to Obtain a Uniform Outlet Temperature

The object of this case is to obtain a uniform or close to uniform outlet temperature distribution for the 1st side flow. The inlet mass flow distribution is adjusted by the optimization method to obtain the targeted outlet temperature distribution, so that it becomes a kind of inverse heat transfer problem. The heat exchanger geometry and the pressure drops are obtained from the optimization in the last section, and the parameters are shown in Tab. 3. In the present study, the longitudinal heat conduction through the fins, plates, and closing bars are neglected. However this effect which could be of interest in the future study. In addition, the proposed mass flow distributions are assumed to be achievable by proper arrangement of the headers and distributors.

**The Equations to be Solved** We consider the 2D problem. The heat exchanger is splitted into $50 \times 50$ units, as shown in Fig. 11, which is idealized from Fig. 7. For each elements, like small heat exchangers, the energy conservation equations 4 and 5 are solved, e.g., for the hatched element, the following equations apply:

$$\begin{aligned} Q^1_{I,J} &= M^1_J c^1_{pI,J}(T^1_{i+1,J} - T^1_{i,J}) \\ &= U_{I,J}A_{I,J}\left(\frac{T^2_{I,j+1}+T^2_{I,j}}{2} - \frac{T^1_{i+1,J}+T^1_{i,J}}{2}\right) \end{aligned} \tag{7}$$

where $M^1_J$ is the mass flow rate at the $J^{th}$ passage of the 1st side flow, $c^1_{pI,J}$ is the heat capacity, $U_{I,J}$ is the overall heat transfer coefficient of element $I$,$J$, and $A_{I,J}$ is the heat transfer area of element $I$,$J$. The superscripts are the side numbers, and the subscripts are the element locations.

One also has for the 2nd side:

$$\begin{aligned} Q^2_{I,J} &= M^2_I c^2_{pI,J}(T^2_{I,j+1} - T^2_{I,j}) \\ &= U_{I,J}A_{I,J}\left(\frac{T^1_{i+1,J}+T^1_{i,J}}{2} - \frac{T^2_{I,j+1}+T^2_{I,j}}{2}\right) \end{aligned} \tag{8}$$

The overall heat transfer coefficients $U$ is calculated from the following equation:


Copyright © 2003 by ASME

Downloaded From: https://proceedings.asmedigitalcollection.asme.org on 06/29/2019 Terms of Use: http://www.asme.org/about-asme/terms-of-use

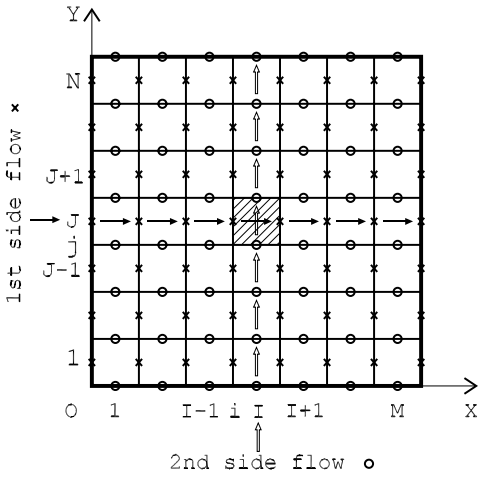


Figure 11. The control volumes for discretization

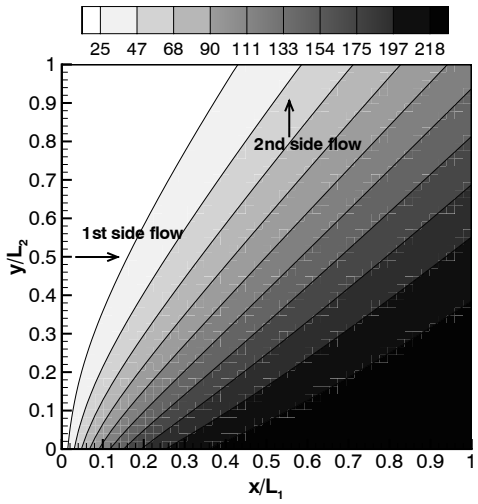


Figure 12. Temperature distribution of the 1st side

$$\frac{1}{UA} = \frac{1}{(\eta_0 hA)_h} + \frac{1}{(\eta_0 hA)_c} \tag{9}$$

where $\eta_0$ is the fin overall efficiency, and $h$ is the heat transfer coefficient calculated as follows,

$$h = \frac{jGc_p}{Pr^{2/3}} \tag{10}$$

where $G$ is the mass flow velocity.

This overall heat transfer coefficient $U$ is calculated for each control volume, because it is not uniform for an uneven flow distribution from the heat exchanger header, i.e., $G$ and $j$ are different for different passages.

By setting $C^1_{I,J} \doteq M^1_J c^1_{pI,J}$, $C^2_{I,J} \doteq M^2_J c^2_{pI,J}$, and $C_{I,J} \doteq U_{I,J}A_{I,J}$, the following equations can be obtained:

$$\begin{aligned}(2C^1_{I,J} + C_{I,J})T^1_{i+1,J} &= (2C^1_{I,J} - C_{I,J})T^1_{i,J} \\ &\quad + C_{I,J}(T^2_{I,j+1} + T^2_{I,j}) \end{aligned} \tag{11}$$

$$\begin{aligned}(2C^2_{I,J} + C_{I,J})T^2_{I,j+1} &= (2C^2_{I,J} - C_{I,J})T^2_{I,j} \\ &\quad + C_{I,J}(T^1_{i+1,J} + T^1_{i,J}) \end{aligned} \tag{12}$$

These are implicit equations, and can be solved by iteration methods.

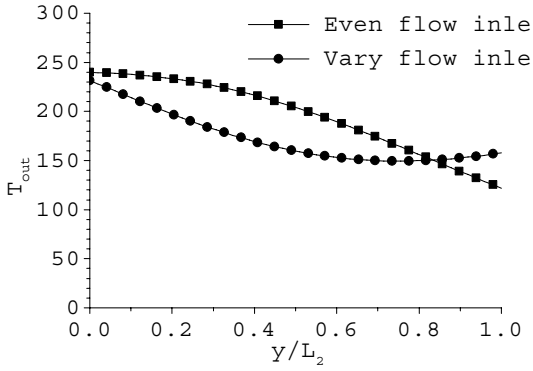


Figure 13. The outlet temperature distribution of the 1st side

**Obtained Temperature Distribution** Figure 12 shows the predicted temperature distribution on the 1st flow side with the uniform mass flow distribution. The temperature distribution at the outlet is shown in Fig. 13. As shown, the difference between the maximum and minimum outlet temperature is about 120 $^{o}$C, which is far from uniform.

**Optimization of the Inlet Mass Flow Distribution** In order to obtain a more uniform outlet temperature, the optimization is directed to minimize the difference $F$ between the outlet temperature distribution and the uniform temperature distribution.


Copyright © 2003 by ASME

Downloaded From: https://proceedings.asmedigitalcollection.asme.org on 06/29/2019 Terms of Use: http://www.asme.org/about-asme/terms-of-use

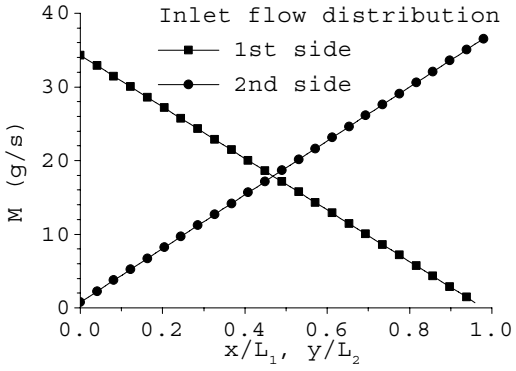


Figure 14. The inlet mass distribution of the two sides

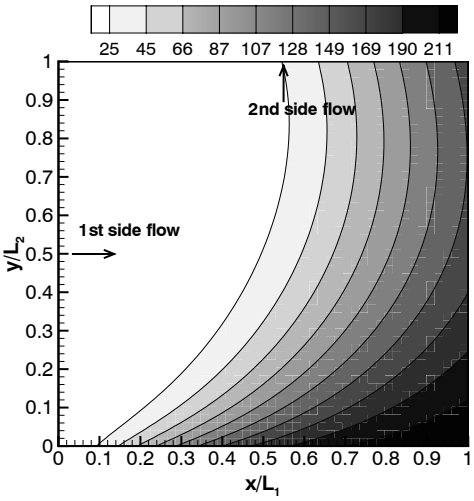


Figure 15. Temperature distribution of the 1st side with varying mass flow distribution

$$F = \sum_{j=1}^{N} \left| T_{M,j} - \overline{T} \right|^2 \tag{13}$$

where $M$, $N$ are the numbers of elements in the $i$, and $j$ direction, respectively, and $\overline{T}$ is the average outlet temperature.

Figure 14 shows the optimized mass flow distribution. As shown, the 1st side mass flow rate decreases with the distance from the 2nd side inlet. Because the exchange of heat between the 2nd side flow with 1st side flow, the temperature difference becomes smaller. Therefore, the flow rate of the 1st side flow should be smaller at the places further from the 2nd side flow inlet. At the same time, the mass flow distribution of the 2nd side flow is also uneven, because stronger flow is preferable to keep the heat exchange ability further downstream.

Figure 15 shows the temperature distribution of the 1st side flow. The outlet temperature distribution, which is shown in Fig. 13, is much more uniform than for the even mass flow inlet. The difference between the largest and smallest is about 80 $^{o}$C. In this optimization, only linear distribution of mass flow inlet is assumed, so the unevenness of the outlet temperature is still large. Nonlinear distribution of the mass flow could also be used, which could provide a more uniform outlet temperature.

The adjustment of the inlet mass flow distribution also results in the degradation of the heat transfer efficiency. For the uniform mass flow inlet, the heat transfer efficiency is 0.8296. However, only 0.716 is obtained if the uneven mass flow inlet is applied. This is because the uneven heat transfer coefficient distribution for the uneven mass flow inlet, as shown in Fig. 16. This is similar to the maldistribution phenomena in heat exchangers, as studied by Ranganayakulu et al. [11].

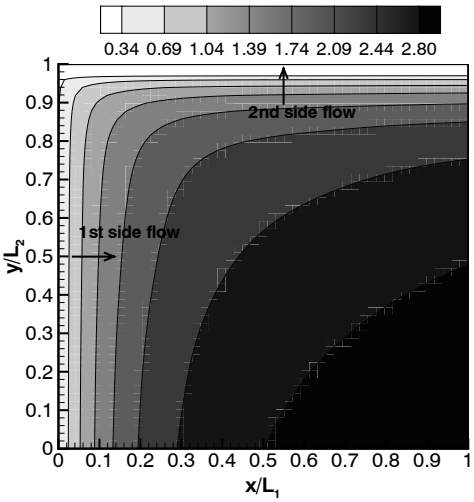


Figure 16. $UA$ distribution with the vary inlet

## CONCLUSIONS

The ANN model used in the present study can accurately predict the heat transfer and friction factors. This also enables the detailed parameter study of compact heat exchangers.

The adopted optimization method is effective in solving the inverse heat transfer problem. However, the resulted temperature distribution is still not satisfactory. Nonlinear mass flow inlet distribution and/or inlet temperature distribution could be employed in future studies.

In addition, a neural network could be constructed and trained by the mass flow distribution and the temperature distri-


Copyright © 2003 by ASME

Downloaded From: https://proceedings.asmedigitalcollection.asme.org on 06/29/2019 Terms of Use: http://www.asme.org/about-asme/terms-of-use

bution of the outlet side where one wants a desired temperature distribution. The temperature distribution is set as the input, and the mass flow distribution is the output. After the training of the neural network, one can give the desired temperature outlet distribution as the input, and then get the mass flow distribution as the output. In this way, the inverse problem can be solved.

## ACKNOWLEDGMENT

The Swedish Energy Agency (STEM) financially supported this research work.

## REFERENCES

[1] Diaz, G., Sen, M., Yang, K.T., and McClain, R.L., 1999, "Simulation of heat exchanger performance by artificial neural networks", *Int. J. HVAC & R. Res* 5(3), pp. 195-208.

[2] Sen, M., and Yang, K.T., 1999, "Applications of artificial neural networks and genetic algorithms in thermal engineering". Editor: F. Kreith, *CRC Handbook of Thermal Engineering*, pp. 620-661.

[3] Kalogirou, S.A., Panteliou, S., and Dentsoras, A., 1999, "Artificial neural networks used for the performance prediction of a thermosyphon solar water heater", *Renewable Energy*, 18(1), pp. 87–99.

[4] Thibault, J., and Grandjean, B.P.A., 1991, "A neural network methodology for heat transfer data analysis", *Int. J. Heat Mass Transfer*, 34(8), pp. 2063-2070.

[5] Mistry, S.I., and Nair, S.S., 1993, "Nonlinear HVAC computations using artificial neural networks". In: *ASHRAE Transactions*, 99(1), pp. 775-784.

[6] Mazzola, A., 1997, "Integrating artificial neural networks and empirical correlations for the prediction of water-subcooled critical heat flux", *Revue Generale de Thermique*, 36(11), pp. 799-806.

[7] Rajkumar, T., Aragon, C., Bardina, J., and Britten, R., 2002, "Prediction of aerodynamic coefficients for wind tunnel data using a genetic algorithm optimized neural network", *7th Int. Conf. High Performance Computing*, Bologna, Italy.

[8] Chouai, A., Laugier, S., and Richon, D., 2002, "Modeling of thermodynamic properties using neural networks: Application to refrigerants", *Fluid Phase Equilibria*, 199(1-2), pp. 53–62.

[9] Dubey, B. P., Pilkhwal, D. S., and Vijayan, P. K., 1998, "Reliable prediction of complex thermal hydraulic parameters by ANN", *Annals of Nuclear Energy*, 25(13), pp. 1069–1078.

[10] Hagan, M.T., Demuth, H.B., and Beale, M., 1996, *Neural Network Design*, ISBN 0-9717321-0-8.

[11] Ranganayakulu, C.H., Seetharamu, K.N., and Sreevatsan, K. V., 1996, "The effects of inlet fluid flow nonuniformity on thermal performance and pressure drops in crossflow plate-fin compact heat exchangers", *Int. J. Heat Mass Transfer*, 40(1), pp. 27–38.

[12] Jia, R., Sundén, B., Xuan, Y., 2001, "Design and optimization of compact heat exchangers", *3rd Int. Con. on Compact Heat Exchangers and Enhancement Technology for the Process Industries*, Eds: Shah, R.K., Davos, Switzerland, pp. 135-142.

[13] Kays, W.M., and London, A.L. 1964, *Compact heat exchangers*, 2nd Edn, McGrawHill Book Co., New York.



Copyright © 2003 by ASME

Downloaded From: https://proceedings.asmedigitalcollection.asme.org on 06/29/2019 Terms of Use: http://www.asme.org/about-asme/terms-of-use